Progress In Electromagnetics Research M, Vol. 28, 185–199, 2013

SEMICONDUCTOR QUANTUM DOT LASERS AS PULSE SOURCES FOR HIGH BIT RATE DATA TRANSMISSION

Mohamed Nady Abdul Aleem[1, *], Khalid F. A. Hussein[2], and Abd-El-hadi A. Ammar[3]

[1]Microwave Engineering Department, Electronics Research Institute, Cairo, Eygpt

[2]Microwave Engineering Department, Electronics Research Institute, Cairo, Eygpt

[3]Electronics and Electrical Communications Department, Faculty of Engineering, El-AZHAR University, Cairo, Eygpt

Abstract—Multi Populations Rate Equations (MPREs) model is used to analyze the dynamic characteristics of the InAs/InP (113) B self assembled quantum dot laser. The resulting system of differentaial equations is solved using fourth-order Runge-Kutta method taking into consideration homogeneous and inhomogeneous broadening of optical gain. The effects of the injected current, Full Width at Half Maximum (FWHM) of the homogenous broadening, and initial relaxation time (phonon bottleneck) on the rise time, fall time, and hence the maximum allowable bit rate of the optical signal are investigated.

1. INTRODUCTION

A critical part of the design of a communication system is the choice of the transmitter or source laser. High bit rate optical time-division multiplexed (OTDM) systems in particular demand reliable short pulse generation at high repetition rates. Semiconductor lasers are becoming increasingly attractive and viable for such applications. Semiconductor lasers can be compact sources of picoseconds, high repetition rate pulses of light at the popular telecommunication wavelength of 1.5 μm [1, 2]. Recent advances in semiconductor processing and cavity design have led to the advent of ultra-stable [3] and ultralow-noise [4]

Received 25 November 2012, Accepted 17 January 2013, Scheduled 22 January 2013

* Corresponding author: Mohamed Nady Abdul Aleem (mnas1000@yahoo.com).

performance. Single-channel, single polarization transmission rates up to 160 Gb/s [5] have been successfully demonstrated using mode-locked semiconductor lasers, and detailed characterization of their noise properties [4] indicate that they may be useful sources for transmission rates beyond 1 Tb/s.

Quantum dot is a new kind of semiconductor nanostructure that confines the movement of carriers in all three dimensions. For this reason, QDs have discrete and finite energy levels and behave like atoms, i.e., the electronic energy is quantized in three dimensions. Compared with traditional bulk laser, quantum well (QW) laser and quantum wire (QWR) laser, the QD laser has many advantages as follows: lower threshold current, temperature insensitivity, very small α-parameter (or linewidth enhancement factor-LEF) and so on [6–8]. Therefore the moment QD laser has been proposed, and more and more researchers are attracted to this area [9, 10, 22]. As a result, thanks to QDs lasers, several steps towards cost reduction can be reached such as improving the laser resistance to temperature fluctuation in order to remove temperature control elements, or designing a feedback resistant laser for isolator-free transmissions and optics-free module.

As mentioned above, semiconductors lasers with quantum dots in their active regions are expected to exhibit many superior properties. However, we know that actual QDs do not always satisfy our expectations because of the energy level broadening (homogeneous broadening) and size distributions (inhomogeneous broadening) and phonon bottleneck. Thus, for an accurate modeling of quantum dot laser diode performance, we must take into account all these actual aspects of QDs [11].

In this paper, first, we describe QD laser analyzing theory based on the multi population rate equations model and consider the homogeneous and inhomogeneous broadening of the optical gain for solving InAs/InP self-assembled quantum dot laser (SAQD-LD) rate equations numerically using fourth-order Runge-Kutta method. Then, in the result section, we study the effect of the FWHM of homogeneous broadening and the injected current on the rise and fall time, hence on the bit rate. Finally, the effects of the initial relaxation oscillation time are treated.

2. MULTI POPULATION RATE EQUATIONS MODEL

In the following, a numerical model is used to study carrier dynamics in the two lowest energy levels of an InAs/InP (113) B QD system. Its active region consists of a QD ensemble, where different dots are interconnected by a wetting layer (WL). For simplicity the existence

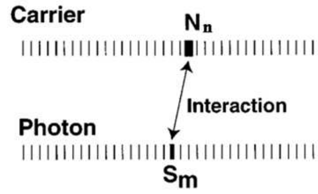

Figure 1. The interaction between the cavity-mode photons and the carriers in the quantum dots via homogeneous broadening of gain.

of higher excited states is neglected and a common carrier reservoir is associated to both the WL and the barrier. In order to include the inhomogeneous broadening of the gain due the dot size fluctuation, and to describe the interaction between the QDs with different resonant energies through photons, we divide the QD ensemble into $2N+1$ groups, depending on their resonant energy for the interband transition; of the ES, $E_{\mathrm{ES}n}$, and of the GS, $E_{\mathrm{GS}n}$. As a result, number of $2M+1$ longitudinal cavity photon modes are constructed in the cavity, as shown in Fig. 1. The index $n=N$ corresponds to the central QD group whereas $m=M$ corresponds to the central mode with the transitional energies E_{ES0} and E_{GS0}. We take the energy width of each group equal to the mode separation between the longitudinal cavity photon modes which can be expressed as [12]

$$\Delta E = ch/2n_r L_{ca}, \tag{1}$$

where L_{ca} is the cavity length, n_r the refractive index, c the speed of light, and h the blank constant.

The energy of the n-th QDs group is represented by

$$E_{\mathrm{ES}n,\mathrm{GS}n} = E_{\mathrm{ES0,GS0}} - (N-n)\,\Delta E, \quad n = 1, 2, \ldots, 2N+1 \tag{2}$$

In the following analysis, QDs are assumed to be always neutral and electrons and holes are treated as eh-pairs and thermal effects and carrier losses in the barrier region are not taken into account. Fig. 2 shows a schematic representation of the carrier dynamics in the conduction band of the n-th QD sub-group in the active region. First, an external carrier injection fills directly the WL reservoir with I being the injected current. Some of the eh-pairs are then captured on the fourfold degenerate ES of the QD ensemble with a capture time $\tau_{\mathrm{ES}n}^{\mathrm{WL}}$. Once on the ES, carriers can relax on the twofold GS within a period of time $\tau_{\mathrm{GS}n}^{\mathrm{ES}}$, they can be thermally reemitted in the WL reservoir $\tau_{\mathrm{WL}n}^{\mathrm{ES}}$ or recombine spontaneously with a spontaneous emission time $\tau_{\mathrm{ES}}^{spon}$ or by stimulated emission of photons with ES resonance energy. The same dynamic behavior is followed for the carrier population in

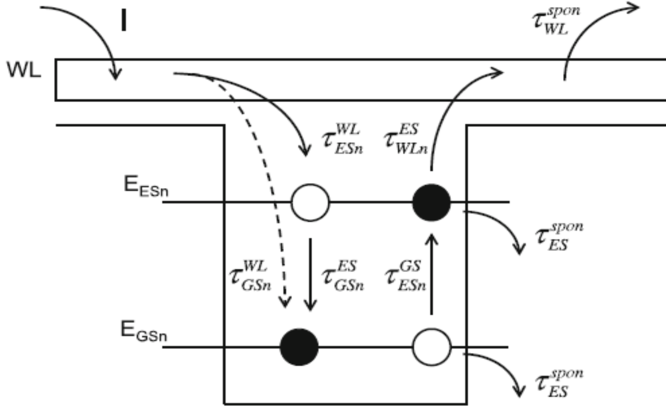

Figure 2. Energy diagram of the laser-active region, diffusion, recombination, and relaxation processes.

the GS with regard to the ES. This approach has been previously developed for the In(Ga)As/GaAs system [12–14] but in the case of InAs/InP (113) B system it is assumed that at low injection rates, the relaxation processes are phonon-assisted while the Auger effect dominates when the injection gets larger [15, 16]. In order to include this effect, a modified model has been considered introducing a direct relaxation channel $\tau_{\mathrm{GS}n}^{\mathrm{WL}}$ to the standard cascade relaxation model as shown in Fig. 2 (dashed line). It is attributed to a single Auger process involving a WL electron captured directly into the GS by transferring its energy to a second WL electron [17]. Carriers are either captured from the WL reservoir into the ES or directly into the GS within the same time $\tau_{\mathrm{GS}n}^{\mathrm{WL}} = \tau_{\mathrm{ES}n}^{\mathrm{WL}}$. This assumption has been made after analysis of the kinetic curves in [15] where the ES and GS populations gave raise simultaneously 10 ps after excitation. On the other hand, carriers can also relax from the ES to the GS with relaxation time $\tau_{\mathrm{GS}n}^{\mathrm{ES}}$. The other transition mechanisms remain the same as in the cascade model.

The capture and the relaxation times are then calculated through a phenomenological relation depending on the carrier density in the WL reservoir [18], the ES and GS occupation probabilities, and the existence probability of the ES and GS transitions

$$\tau_{\mathrm{ES}n}^{\mathrm{WL}} = \frac{1}{(A_w + (C_w N_{\mathrm{WL}})/V_{\mathrm{WL}})\,(1 - P_{\mathrm{ES}n}) G_{n\mathrm{ES}}} \tag{3}$$

$$\tau_{\mathrm{GS}n}^{\mathrm{ES}} = \frac{1}{(A_E + (C_E N_{\mathrm{WL}})/V_{\mathrm{WL}})\,(1 - P_{\mathrm{GS}n})} \tag{4}$$

$$\tau_{\mathrm{GS}n}^{\mathrm{WL}} = \frac{1}{\left(A_w + (C_w N_{\mathrm{WL}})/V_{\mathrm{WL}}\right)(1 - P_{\mathrm{GS}n}) G_{n\mathrm{GS}}} \tag{5}$$

where N_{WL} is the carrier number in the WL reservoir, V_{WL} is the WL volume and $A_w(A_E)$, $C_w(C_E)$ are the coefficients for phonon and Auger-assisted relaxation, respectively, related to the WL (ES). $P_{\mathrm{ES}n}$ and $P_{\mathrm{GS}n}$ are the filling probabilities of the ES and GS, respectively, in the nth subgroup of dots given by

$$P_{\mathrm{ES}n} = \frac{N_{\mathrm{ES}n}}{\mu_{\mathrm{ES}} N_d w L_{ca} N_l G_{n\mathrm{ES}}}, \quad P_{\mathrm{GS}n} = \frac{N_{\mathrm{GS}n}}{\mu_{\mathrm{GS}} N_d w L_{ca} N_l G_{n\mathrm{GS}}} \tag{6}$$

where $N_{\mathrm{ES}n}$, $N_{\mathrm{GS}n}$ being the ES and GS carrier number in the nth subgroup, μ_{ES}, μ_{GS} are the degeneracy of the considered confined states, N_d is the QD surface density, w and L_{ca} are the width and length of the active region, and N_l being the number of QD layers. $G_{n\mathrm{ES}}$ and $G_{n\mathrm{GS}}$ are the probabilities of recombination with $E_{\mathrm{ES}n}$ and E_{GSn} energy, respectively. To calculate them, a Gaussian QD size distribution has been considered with a consequent Gaussian distribution of the QD recombination energies.

$$G_{n\mathrm{ES},n\mathrm{GS}} = \frac{1}{\sqrt{2\pi}\chi_0} \exp\left(E_{n\mathrm{ES},n\mathrm{GS}} - E_{\mathrm{ES0,GS0}}\right)^2 / 2\chi_0^2, \tag{7}$$

where the FWHM of the inhomogeneous broadening is given by $\Gamma_0 = 2.35\chi_0$.

The eh-pairs escape times have been derived considering a Fermi distribution for the ES and GS carriers for the system in quasi-thermal equilibrium without external excitation [19]. To ensure this, the carrier escape time is related to the carrier capture time as follows:

$$\tau_{\mathrm{ES}n}^{\mathrm{GS}} = \tau_{\mathrm{GS}n}^{\mathrm{ES}} \frac{\mu_{\mathrm{GS}}}{\mu_{\mathrm{ES}}} e^{(E_{\mathrm{ES}n} - E_{\mathrm{GS}n})/K_B T} \tag{8}$$

$$\tau_{\mathrm{WL}n}^{\mathrm{ES}} = \tau_{\mathrm{ES}n}^{\mathrm{WL}} \frac{\mu_{\mathrm{ES}} N_d N_l}{\rho_{\mathrm{WL}\mathit{eff}}} e^{(E_{\mathrm{WL}} - E_{\mathrm{ES}n})/K_B T} \tag{9}$$

$$\tau_{\mathrm{WL}n}^{\mathrm{GS}} = \tau_{\mathrm{GS}n}^{\mathrm{WL}} \frac{\mu_{\mathrm{GS}} N_d N_l}{\rho_{\mathrm{WL}\mathit{eff}}} e^{(E_{\mathrm{WL}} - E_{\mathrm{GS}n})/K_B T} \tag{10}$$

where ($\rho_{\mathrm{WL}\mathit{eff}} = m_{e\mathrm{WL}} K_B T / \pi\hbar^2$) [20] is the effective density of states in the WL and E_{WL} is its emission energy. The numerical model is based on the MPRE analysis already reported in [21]. According to all those assumptions the MPRE system, describing the change in carrier number of the three electronic energy levels; WL, ES, and GS, can be written as

$$\frac{dN_{\mathrm{WL}}}{dt} = \frac{I}{e} + \sum_n \frac{N_{\mathrm{ES}n}}{\tau_{\mathrm{WL}n}^{\mathrm{ES}}} + \sum_n \frac{N_{\mathrm{GS}n}}{\tau_{\mathrm{WL}n}^{\mathrm{GS}}} - \frac{N_{\mathrm{WL}}}{\tau_{\mathrm{ES}}^{\mathrm{WL}}} - \frac{N_{\mathrm{WL}}}{\tau_{\mathrm{WL}}^{spon}} - \frac{N_{\mathrm{WL}}}{\tau_{\mathrm{GS}}^{\mathrm{WL}}} \tag{11}$$

$$\frac{dN_{\mathrm{ES}n}}{dt} = \frac{N_{\mathrm{WL}}}{\tau_{\mathrm{ES}n}^{\mathrm{WL}}} + \frac{N_{\mathrm{GS}n}\left(1-P_{\mathrm{ES}n}\right)}{\tau_{\mathrm{ES}n}^{\mathrm{GS}}} - \frac{N_{\mathrm{ES}n}}{\tau_{\mathrm{WL}n}^{\mathrm{ES}}} - \frac{N_{\mathrm{ES}n}}{\tau_{\mathrm{GS}n}^{\mathrm{ES}}} - \frac{N_{\mathrm{ES}}}{\tau_{\mathrm{ES}}^{spon}} - \frac{c\Gamma}{n_r}\sum_m g_{mn\mathrm{ES}} S_m \tag{12}$$

$$\frac{dN_{\mathrm{GS}n}}{dt} = \frac{N_{\mathrm{WL}}}{\tau_{\mathrm{GS}n}^{\mathrm{WL}}} + \frac{N_{\mathrm{ES}n}}{\tau_{\mathrm{GS}n}^{\mathrm{ES}}} - \frac{N_{\mathrm{GS}n}\left(1-P_{\mathrm{ES}n}\right)}{\tau_{\mathrm{ES}n}^{\mathrm{GS}}} - \frac{N_{\mathrm{GS}n}}{\tau_{\mathrm{WL}n}^{\mathrm{GS}}} - \frac{N_{\mathrm{GS}}}{\tau_{\mathrm{GS}}^{spon}} - \frac{c\Gamma}{n_r}\sum_m g_{mn\mathrm{GS}} S_m \tag{13}$$

with n_r being the refractive index and Γ is the optical confinement factor.

In order to calculate the entire emission spectrum, the model has been extended considering also the presence of many cavity longitudinal modes, Fig. 1, hence the photon number with resonant energy of the mth mode is depicted by

$$\frac{dS_{\mathrm{ES}m}}{dt} = \frac{c\Gamma}{n_r}\sum_n g_{mn\mathrm{ES}} S_{\mathrm{ES}m} - \frac{S_{\mathrm{ES}m}}{\tau_p} + \beta\sum_n\left(B_{\mathrm{ES}}(E_m - E_{\mathrm{ES}n})\,\frac{N_{\mathrm{ES}}}{\tau_{\mathrm{ES}}^{spon}}\right)\Delta E_m \tag{14}$$

$$\frac{dS_{\mathrm{GS}m}}{dt} = \frac{c\Gamma}{n_r}\sum_n g_{mn\mathrm{GS}} S_{\mathrm{GS}m} - \frac{S_{\mathrm{GS}m}}{\tau_p} + \beta\sum_n\left(B_{\mathrm{GS}}(E_m - E_{\mathrm{GS}n})\,\frac{N_{\mathrm{GS}}}{\tau_{\mathrm{ES}}^{spon}}\right)\Delta E_m \tag{15}$$

where $S_{\mathrm{ES}m}$ and $S_{\mathrm{GS}m}$ are the number of photons emitted from exited and ground state at the mode number m, respectively, and S_m is the total number of photons at the mth mode which equals to $S_m = S_{\mathrm{ES}m} + S_{\mathrm{GS}m}$. The rate of photons emitted out of the cavity is $\frac{S_{\mathrm{ES}m}}{\tau_p}$ and $\frac{S_{\mathrm{GS}m}}{\tau_p}$, with $(\tau_p = 1/[V_g(\alpha_i + \frac{In(1/R_1R_2)}{2L_{ca}})]$ being the photon lifetime [21]. The contribution of the spontaneous emission to the lasing mode is calculated as the ES and GS spontaneous transitions multiplied by the spontaneous emission coupling factor β, assumed to be constant. In Equations (12)–(15), the material gain is described by the set of equations

$$g_{mn\mathrm{ES}} = \mu_{\mathrm{ES}}\frac{\pi e^2\hbar}{cn_r\varepsilon_0 m_0^2}\frac{N_d}{H}\frac{\left|P_{\mathrm{ES}}^{\sigma}\right|^2}{E_{\mathrm{ES}n}}\times(2P_{\mathrm{ES}n}-1)\,G_{n\mathrm{ES}}B_{\mathrm{ES}}(E_{\mathrm{ES}m}-E_{\mathrm{ES}n}) \tag{16}$$

$$g_{mn\mathrm{GS}} = \mu_{\mathrm{GS}} \frac{\pi e^2 \hbar}{c n_r \varepsilon_0 m_0^2} \frac{N_d}{H} \frac{|P_{\mathrm{GS}}^{\sigma}|^2}{E_{\mathrm{GS}n}} \times (2P_{\mathrm{GS}n} - 1)\, G_{n\mathrm{GS}} B_{\mathrm{GS}}(E_{\mathrm{GS}m} - E_{\mathrm{GS}n}) \tag{17}$$

where H is the average height of the QD and $|P_{\mathrm{ES,GS}}^{\sigma}|$ the density matrix momentum [22] given by

$$|P_{cv}^{s}|^2 = |I_{cv}|^2 M^2, \tag{18}$$

where I_{cv} represents the overlap integral between the envelope functions of an electron and a hole; which is taken equal to one, and

$$M^2 = \frac{m_0^2}{12 m_e^*} \frac{E_g(E_g + \Delta)}{E_g + 2\Delta/3}, \tag{19}$$

where E_g is the band gap, m_e^* the electron effective mass, and Δ the spin-orbit interaction energy of the QD material [22].

Furthermore, let us emphasize that the various QD population are coupled by the homogeneous broadening of the stimulated emission process assumed to be Lorentzian such as

$$B_{\mathrm{ES,GS}}\left(E_{\mathrm{ES}m,\mathrm{GS}m} - E_{\mathrm{ES}n,\mathrm{GS}n}\right) = \frac{\Gamma_{hom}/2\pi}{\left(E_{\mathrm{ES}m,\mathrm{GS}m} - E_{\mathrm{ES}n,\mathrm{GS}n}\right)^2 + \left(\Gamma_{hom}/2\pi\right)^2} \tag{20}$$

with Γ_{hom} being the full-width at half-maximum (FWHM) of the homogeneous broadening and ($E_{\mathrm{ES}m,\mathrm{GS}m} = E_{\mathrm{ES0,GS0}} - (M - m)\Delta E$) being the mode energy. All parameters used in the calculations are summarized in Table 1.

3. NUMERICAL RESULTS

The Multi Populations Rate Equations MPRE model together with the photons rate Equations (11)–(15) have been solved using the fourth order Runge-Kotta method with the help of the optical gain Equations (16), (17). In this section, the effect of the injected current, the FWHM of homogeneous broadening, and phonon bottleneck on the rise time, fall time, and the bit rate will be treated.

Figure 3 shows the simulation results of photon-characteristics when the inhomogeneous broadening is neglected, $N = M = 0$. In this figure the normalized number of photons (normalized to its maximum) and the injected current pulse are plotted versus time. The results of Fig. 3 represent the ideal case which cannot practically be realized. As seen in this figure, the rise time is exactly equal to the turnon delay and the time of the relaxation oscillations which is less than 20 psec. On the other hand, the fall time is negligible as it is less than 10 psec.

Table 1. Parameters used for simulation of InAs/InP (113) B quantum dot laser.

Parameter		Value
E_{WL}	Emission energy of the WL	$1.05\,\mathrm{eV}$
$\tau_{\mathrm{ES}}^{spon}$	Spontaneous emission from ES	$500\,\mathrm{ps}$
$\tau_{\mathrm{GS}}^{spon}$	Spontaneous emission from GS	$1200\,\mathrm{ps}$
$\tau_{\mathrm{WL}}^{spon}$	Spontaneous emission from WL	$500\,\mathrm{ps}$
A_w	WL phonon assisted relaxation	$1.35 \times 10^{10}\,\mathrm{s}^{-1}$
A_E	ES phonon assisted relaxation	$1.5 \times 10^{10}\,\mathrm{s}^{-1}$
C_w	WL Auger coefficient	$5 \times 10^{-15}\,\mathrm{m}^3\mathrm{s}^{-1}$
C_E	ES Auger coefficient	$9 \times 10^{-14}\,\mathrm{m}^3\mathrm{s}^{-1}$
E_{ES0}	ES central energy transition	$0.840\,\mathrm{eV}$
E_{GS0}	GS central energy transition	$0.792\,\mathrm{eV}$
R	Average QD radius	$1.55 \times 10^{-6}\,\mathrm{cm}$
H	Average QD hight	$2 \times 10^{-7}\,\mathrm{cm}$
ND	QD Surface density	$10^{11}\,\mathrm{cm}^2/\mathrm{QD}$ layer
NW	Number of QD layers	6
Γ	Optical Confinement factor	0.036
$R_1 = R_2$	Mirror reflectively	0.33
α_i	Cavity internal loss	$10\,\mathrm{cm}^{-1}$

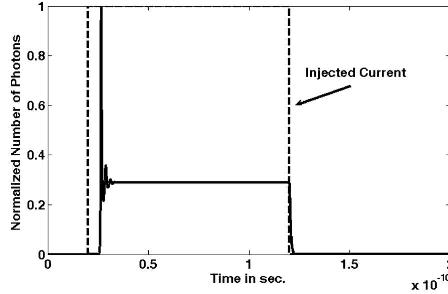

Figure 3. Normalized photon-characteristics at $N = M = 0$ and current density; $J = 180\,\mathrm{A/cm}^2$.

In the following investigations, the number of groups as well as the number of modes are set to 15, i.e., $N = M = 7$. Fig. 4 shows the normalized number of photons versus time at $\Gamma_0 = 20\,\mathrm{meV}$, $\Gamma_{hom} = 10\,\mathrm{meV}$ and at different injected current densities; $J = 100$, 250, 500,

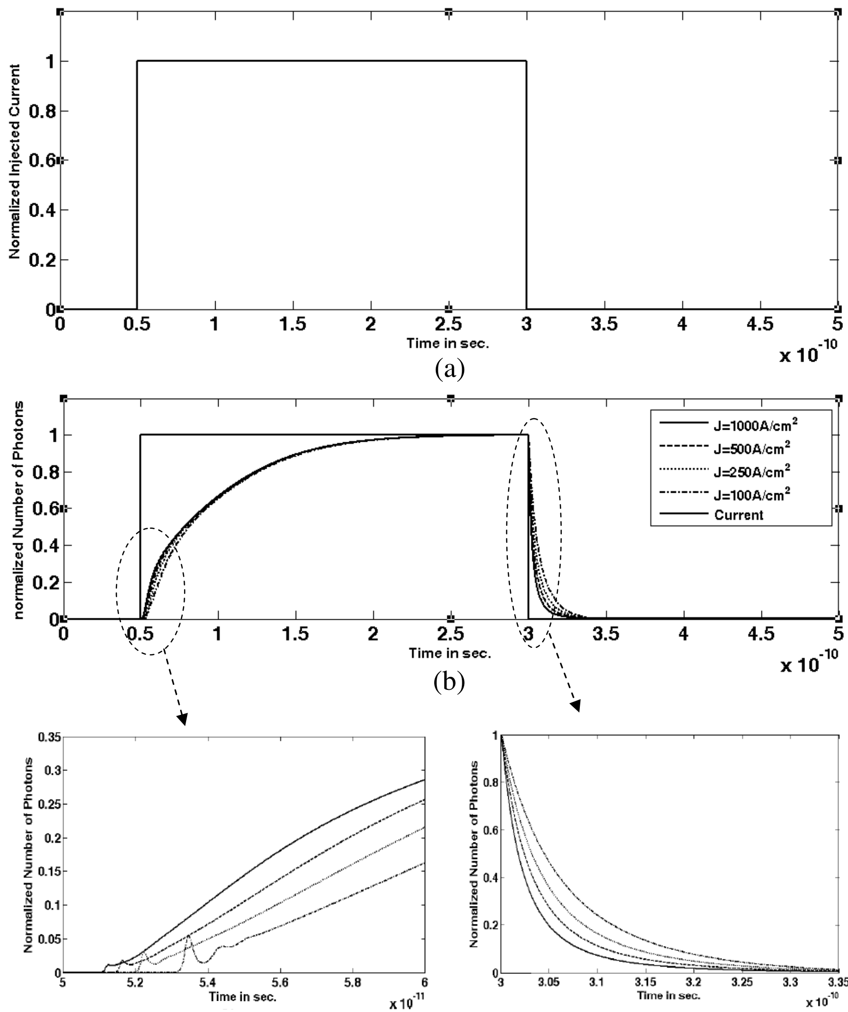

Figure 4. (a) Normalized injected current pulse, (b) photon-characteristics at $\Gamma_0 = 20\,\text{meV}$, $\Gamma_{hom} = 10\,\text{meV}$ and $J = 100$, 250, 500, and $1000\,\text{A/cm}^2$.

and $1000\,\text{A/cm}^2$. as shown in Fig. 4, the current injected takes the form of a square pulse of width 250 psec.

It is shown in the figure that, as the injected current increases the rise time increases whereas the fall time decreases. And it is also shown that, the rate of increase of the number of photons during the rise time is much smaller than the rate of decrease of the number of photons during the fall time.

If we consider that an injected current pulse represents a logic "1" whereas the absence of the current pulse represents a logic "0", then the bit duration is the time duration of the injected current pulse. If a stream of bits is represented by successive current pulses, the rise and fall times of the signal will limit the speed of transmission. It is known that, the bit rate is the inverse of the bit duration and the minimum bit duration (corresponds to the maximum bet rate), in this work, is taken equal to the summation of the rise time with the fall time. Therefore, the maximum possible bit rate increases with increasing the injected current amplitude.

All the above can be explained by that as the current increases the number of carriers supplied to the active region required to start lasing is reached faster and the turn-on delay decreases. As a result, the rise time decreases.

On the other hand, for high current, when the current is switched off, the number of existing carriers is high enough to increase the rate of stimulated emission and as a result, the fall time decreases.

Figure 5 shows dependence of the rise, fall time and bet rate on the injected current. As can be seen from this figure, as the injected current increases the rise time increases while the fall time decreases. The rate of increasing the rise time is small with respect to the rate of the decreasing the fall time. Therefore, the bit rate increases with the increase of the injected current.

To demonstrate the effect of reducing the homogenous broadening on the rise and fall time, the number of generated photons is plotted against time for $\Gamma_{hom} = 0.1\,\text{meV}$ as shown in Fig. 6.

In comparison to the case presented in Fig. 4, it is found that the

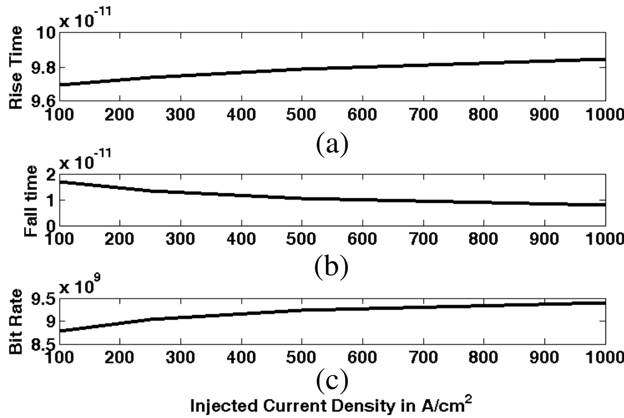

Figure 5. Depends of (a) the rise time, (b) fall time of the number of photons, and (c) bit rate on the injected current at $\Gamma_0 = 20\,\text{meV}$, $\Gamma_{hom} = 10\,\text{meV}$.

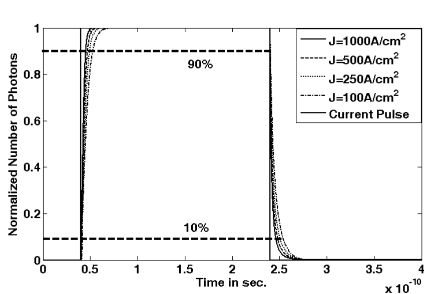

Figure 6. Photon-characteristics at $\Gamma_0 = 20\,\text{meV}$, $\Gamma_{hom} = 0.1\,\text{meV}$ and Current Density $J = 100$, 250, 500, and $1000\,\text{A/cm}^2$.

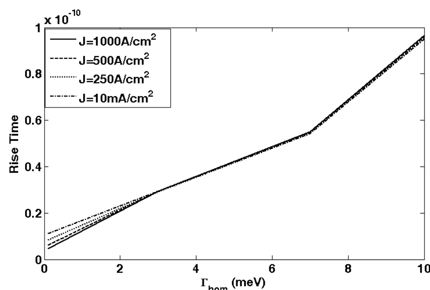

Figure 7. Rise time versus the Homogenous broadening factor; Γ_{hom} at different injected current.

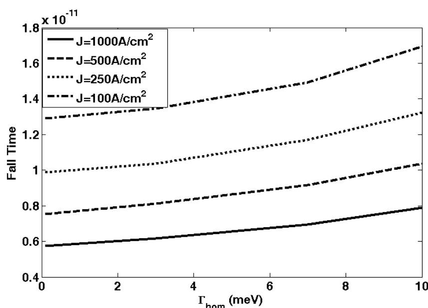

Figure 8. Fall time versus the Homogenous broadening factor; Γ_{hom} at different injected current.

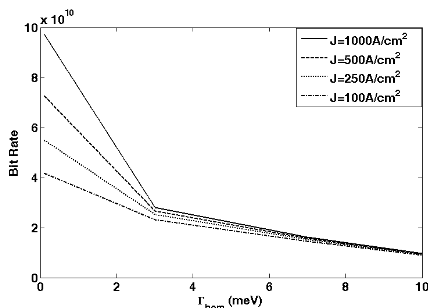

Figure 9. Bit rate versus the Homogenous broadening factor; Γ_{hom} at different injected current.

number of generated photons reaches its steady state faster and hence the rise and fall times are smaller for lower FWHM of the homogenous broadening.

Figures 7, 8 and 9 show the dependence of the rise time, fall time, and the bit rate on the FWHM of the homogenous broadening, Γ_{hom}. In these results, the current density is used as a parameter and its value are; $J = 1000, 500, 250, 100\,\text{A/cm}^2$. Again, these figures explain that, as the Γ_{hom} increases, the rise and fall times increase. Hence, the bit rate decreases.

These results can be explained by considering the effect of the homogeneous broadening of the optical gain of a single dot. When the homogeneous broadening is negligible with respect to the inhomogeneous broadening, dots with different energies have no

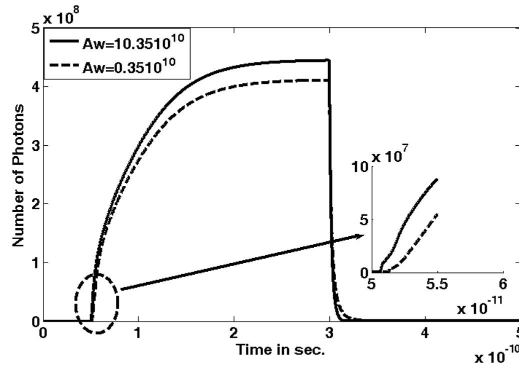

Figure 10. Photon-characteristics at $\Gamma_0 = 20\,\mathrm{meV}$ and $\Gamma_{hom} = 10\,\mathrm{meV}$ and current density CD $= 1000\,\mathrm{A/cm^2}$ at different coefficient for phonon relaxation (Aw).

correlation to each other since they are spatially isolated from each other.

Then, all dots that have an optical gain above the lasing threshold start lasing independently, leading to broad-band lasing emission and they reach the steady state and decay independently with no influence of any group on the others. The quantum-dot laser at this situation behaves in the 15 same way as if it included independent lasing media in the same cavity. When homogeneous broadening is comparable to inhomogeneous broadening, lasing mode photons are emitted not only from energetically resonant dots, central group, but also from other non resonant dots within the scope of the homogeneous broadening of the central group. Since carriers of non resonant dots are brought into the central lasing mode by stimulated emission, lasing emission with a narrow line takes place and the time to reach steady state and decay time of the lasing mode will be slower [16].

The final result is the study of the initial carrier relaxation which corresponds to phonon bottleneck. Fig. 10 shows the photon-characteristics at $\Gamma_0 = 20\,\mathrm{meV}$ and $\Gamma_{hom} = 10\,\mathrm{meV}$ and Current Density CD $= 100\,\mathrm{A/cm^2}$ at different coefficient for phonon relaxation; Aw $= 0.35 * 10^{10}$, and $10.35 * 10^{10}\mathrm{s^{-1}}$.

As shown in Fig. 10, as the Aw coefficient decreases which means the initial carrier relaxation time increases, referred to Equations (3), (5), the turn on delay increases and the steady state value becomes lower. This is because, the injected carriers are consumed in the WL and thus do not contribute to lasing oscillation. It can be seen also that, the effect of this parameter on the rise and fall time is weak. To see this effect, we plot in Fig. 11 the dependence

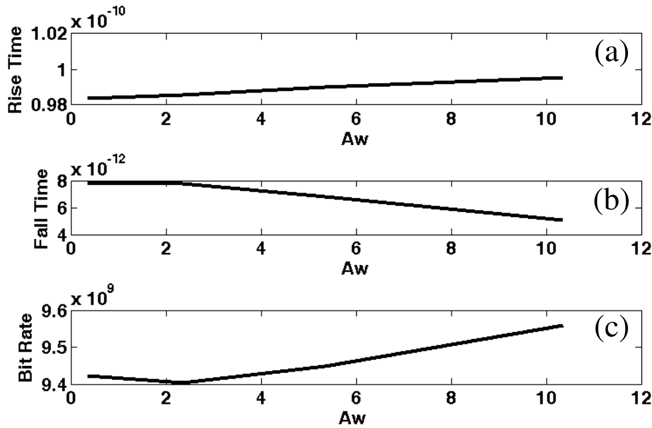

Figure 11. (a) Rise, (b) fall time and (c) bit rate versus the coefficient of phonon relaxation (Aw) at $\Gamma_0 = 20\,\text{meV}$, $\Gamma_{hom} = 10\,\text{meV}$.

of rise and fall time and the bit rate on the Aw coefficient.

As can be seen, the rise time increases and the fall time decrease as the Aw coefficient increases. As a result, the bit rate increases. These results can be explained by noting that, the effect of increasing Aw coefficient is equivalent to the increase of the injected current, which means increasing the supplied carriers to the QD region.

4. CONCLUSIONS

Considering the homogeneous and inhomogeneous broadening of the optical gain, we solved the Multi Populations Rate Equations MPRE numerically using fourth-order Runge-Kutta method and analyzed the effect of the injected current, the FWHM of the homogenous broadening, and the initial relaxation (phonon bottleneck) on the rise, fall time, and the bit rate of the optical pulse. It is founded that, as the injected current increases the rise time increases while the fall time decreases. As a result, the bit rate of the optical pulse increases. With respect to the FWHM of the homogenous broadening Γ_{hom}, as the Γ_{hom} increases, the rise and fall times increase. Consequently, the bit rate decreases. Finally, we find that, the effect of Aw parameter, which related to the initial carrier relaxation time, on the rise and fall time is weak. And the effect of increasing it is equivalent to the increase of the injected current, which means increasing the supplied carriers to the QD region.

REFERENCES

1. Ludwig, R., S. Diez, A. Ehrhardt, L. Küller, W. Pieper, and H. G. Weber, "A tunable femto-second mode locked semiconductor laser for applications in OTDM-systems," *IEICE Trans. on Electron.*, Vol. E81-C, 140–145, 1998.
2. Yokoyama, H., "Highly stabilized mode-locked semiconductor diode lasers," *Rev. Laser Eng.*, Vol. 27, 750–755, 1999.
3. Yokoyama, H., "Highly reliable mode-locked semiconductor lasers," *IEICE Trans. on Electron.*, Vol. E85-C, No. 1, 27–36, 2002.
4. Jiang, L. A., M. E. Grein, E. P. Ippen, C. McNeilage, J. Searls, and H. Yokoyama, "Quantum limited noise performance of a mode locked laser diode," *Opt. Lett.*, Vol. 27, No. 1, 49–51, 2002.
5. Feiste, U., R. Ludwig, C. Schubert, J. Berger, C. Schmidt, H. G.Weber, B. Schmauss, A. Munk, B. Buchold, D. Briggmann, F. Kueppers, and F. Rumpf, "160 Gbit/s transmission over 116 km field-installed fiber using 160 Gbit/s OTDM and 40 Gbit/s ETDM," *Electron. Lett.*, Vol. 37 No. 7, 443–445, 2001.
6. Agrawal, G. P., *Fiber-Optic Communication Systems*, Wiley, New York, 2002.
7. Ramamurthy, B., "Switches, wavelength routers, and wavelength converters," *Optical WDM Networks — Principles and Practice*, K. M. Sivalingam and S. Subramaniam (eds)., 51–75, Kluwer, Boston, 2001.
8. Mukherjee, B. and H. Zang, "Introduction survey of state-of-the-art," *Optical WDM Networks — Principles and Practice*, K. M. Sivalingam and S. Subramaniam (eds.), 3–24, Kluwer, Boston, 2001.
9. Rafailov, E. U., M. A. Cataluna, and E. A. Avrutin, *Ultrafast Lasers Based on Quantum Dot Structures: Physics and Devices*, Wiley, New York, 2011.
10. Sugawara, M., R. K. Willardson, and E. R. Weber, *Self-Assembled InGaAs/GaAs Quantum Dots (Semiconductors and Semimetals)*, Academic Press, 1999.
11. Sugawara, M., N. Hatori, H. Ebe, Y. Arakawa, T. Akiyama, K. Otsubo, and Y. Nakata, "Modelling room-temperature lasing spectra of 1.3 mm homogeneous broadening of optical gain under current injection," *J. Appl. Phy.*, Vol. 97, No. 4, 043523, 2005.
12. Naeimi, A. S., D. G. Nahri, and S. A. Kazemipour, "Analysis of dynamic characteristics of self-assembled quantum dot lasers," *World Applied Sciences Journal*, Vol. 11, No. 1, 6–11, 2010.

13. Sugawara, M., K. Mukai, and Y. Nakata, "Light emission spectra of columnar-shaped self-assembled InGaAs/GaAs quantum-dot lasers: Effect of homogeneous broadening of the optical gain on lasing characteristics," *Appl. Phys. Lett.*, Vol. 74, No. 11, 1999.
14. Markus, A., J. X. Chen, C. Paranthoen, A. Fiore, C. Platz, and O. Gauthier-Lafaye, "Simultaneous two-state lasing in quantum-dot lasers," *Appl. Phys. Lett.*, Vol. 82, No. 12, 1818–1820, 2003.
15. Miska, P., C. Paranthoen, J. Even, O. Dehaese, H. Folliot, N. Bertru, S. Loualiche, M. Senes, and X. Marie, "Optical spectroscopy and modeling of double-cap grown InAs/InP quantum dots with long wavelength emission," *Semicond. Sci. Technol.*, Vol. 17, L63–L67, 2002.
16. Grillot, F., K. Veselinov, M. Gioannini, I. Montrosset, J. Even, R. Piron, E. Homeyer, and S. Loualiche, "Spectral analysis of 1.55 μm InAs-InP (113) B quantum-dot lasers based on a multipopulation rate equations model," *IEEE Journal of Quantum Electronics*, Vol. 45, No. 7, 872–878, 2009.
17. Ohnesorge, B., M. Albrecht, J. Oshinowo, Y. Arakawa, and A. Forchel, "Rapid carrier relaxation in self-assembled $\mathrm{In}_x\mathrm{Ga}_{1-x}$ As/GaAs quantum dots," *Phys. Rev. B*, Vol. 54, No. 16, 11532, 1996.
18. Berg, T., S. Bischoff, I. Magnusdottir, and J. Mork, "Ultrafast gain recovery and modulation limitations in self assembled quantum-dot devices," *IEEE Photonics Technol. Lett.*, Vol. 13, No. 6, 541–543, 2001.
19. Markus, A., J. X. Chen, O. Gauthier-Lafaye, J. Provost, C. Paranthoën, and A. Fiore, "Impact of intraband relaxation on the performance of a quantum-dot laser," *IEEE J. Sel. Topics Quantum Electron.*, Vol. 9, No. 5, 1308–1314, 2003.
20. Gioannini, M. and I. Montrosset, "Numerical analysis of the frequency chirp in quantum-dot semiconductor lasers," *IEEE Journal of Quantum Electronics*, Vol. 43, No. 10, 2007.
21. Gioannini, M., A. Sevega, and I. Montrosset, "Simulations of differential gain and linewidth enhancement factor of quantum dot semiconductor lasers," *Opt. Quantum Electron.*, Vol. 38, No. 4, 381–394, 2006.
22. Farghal, A. E., S. Wageh, and A. E.-S. Abou-El-Azm, "The effect of electrode materials on the optical characteristics of infrared quantum dot-light emitting devices," *Progress In Electromagnetics Research C*, Vol. 19, 47–59, 2011.